© The American Society of Gene & Cell Therapy

Widespread and Efficient Transduction of Spinal Cord and Brain Following Neonatal AAV Injection and Potential Disease Modifying Effect in ALS Mice

Jacob I Ayers[1], Susan Fromholt[1], Olga Sinyavskaya[1], Zoe Siemienski[1], Awilda M Rosario[1], Andrew Li[1], Keith W Crosby[1], Pedro E Cruz[1], Nadia M DiNunno[1], Christopher Janus[1], Carolina Ceballos-Diaz[1], David R Borchelt[1], Todd E Golde[1], Paramita Chakrabarty[1] and Yona Levites[1].

[1]*Department of Neuroscience, Center for Translational Research in Neurodegenerative Disease and McKnight Brain Institute, College of Medicine, University of Florida, Gainesville, Florida, USA*

The architecture of the spinal cord makes efficient delivery of recombinant adeno-associated virus (rAAV) vectors throughout the neuraxis challenging. We describe a paradigm in which small amounts of virus delivered intraspinally to newborn mice result in robust rAAV-mediated transgene expression in the spinal cord. We compared the efficacy of rAAV2/1, 2/5, 2/8, and 2/9 encoding EGFP delivered to the hindlimb muscle (IM), cisterna magna (ICM), or lumbar spinal cord (IS) of neonatal pups. IS injection of all four capsids resulted in robust transduction of the spinal cord with rAAV2/5, 2/8, and 2/9 vectors appearing to be transported to brain. ICM injection resulted in widespread expression of EGFP in the brain, and upper spinal cord. IM injection resulted in robust muscle expression, with only rAAV2/8 and 2/9 transducing spinal motor and sensory neurons. As proof of concept, we use the IS paradigm to express murine Interleukin (IL)-10 in the spinal cord of the SOD1-G93A transgenic mouse model of amyotrophic lateral sclerosis. We show that expression of IL-10 in the spinal axis of SOD1-G93A mice altered the immune milieu and significantly prolonged survival. These data establish an efficient paradigm for somatic transgene delivery of therapeutic biologics to the spinal cord of mice.

Received 4 June 2014; accepted 9 September 2014; advance online publication 4 November 2014. doi:10.1038/mt.2014.180

INTRODUCTION

Despite impressive advances in our understanding of the etiology of neurodegenerative disorders, there has been no success, to date, in translating this knowledge into disease-modifying therapies.[1] In general, therapeutic discovery for central nervous system (CNS) disorders is challenging because of the issues relating to efficient delivery of therapeutic agents to the CNS. Moreover, preclinical target validation studies using traditional transgenic overexpression or knockout models are resource- and time-intensive and prone to confounds from developmental effects of the manipulation. Multiple independent groups have established the utility of recombinant adeno-associated viral (rAAV) vector mediated gene expression as a highly effective tool to model various aspects of neurodegenerative disorders, conduct target validation studies, and evaluate novel therapeutic approaches for CNS diseases.[2–9] By being resource- and time-efficient, rAAV mediated gene targeting serves as a technology accelerator for preclinical animal modeling and therapeutic intervention studies. Moreover, as rAAV vectors have shown promise as efficient and safe gene therapy delivery systems for human clinical studies, especially those targeting the CNS, rAAV vectors that show disease modifying effects in preclinical models may serve as the initial proof of concept for the development of rAAV-based therapeutics.[10,11]

We have previously shown that rAAV-mediated delivery of transgenes via intracerebroventricular injection to newborn mice results in widespread and long-term transgene expression throughout the adult mouse brain.[12] Our intracerebroventricular data show that viral transduction is dependent on the capsid and the developmental stage of the targeted tissue in rodents. For example, intracerebroventricular injection of rAAV2/1 vectors on neonatal day P0 almost exclusively transduce neurons, whereas rAAV2/5 vectors almost exclusively transduce astrocytes.[12] Further, rAAV2/1 injection on neonatal day P2–P3 show mostly choroid restricted brain transduction, whereas rAAV2/8 or 2/9 still display widespread brain transduction, but with preferential astrocyte tropism. Similarly, intravascular injection of rAAV9 targets astrocytes in adult spinal cord but shows high neurotropism in neonatal spinal cord.[13]

Efficient delivery of transgenes to the spinal cord is essential toward modeling and exploring disease modifying therapies in motor neuron diseases (MNDs) or in mouse models of neurodegenerative disease that develop spinal cord pathology and motor phenotypes. In particular, establishing non-invasive and high efficiency gene therapy paradigms targeting the spinal cord are critical for possible future efforts aimed at clinical translation. Toward that end, we have evaluated how various viral delivery routes affect the spinal cord and brain transduction properties of four commonly used rAAV serotypes: rAAV2/1, 2/5, 2/8, and 2/9. By far the most effective of the delivery routes is direct injection of the rAAV vector to the lumbar spinal cord (IS) of newborn mice,

Correspondence: *Paramita Chakrabarty, Center for Translational Research in Neurodegenerative Disease, College of Medicine, University of Florida, 1275 Center Drive, BMS J-496, P.O. Box 100159, Gainesville, Florida 32610, USA. E-mail: pchakrabarty@ufl.edu or Yona Levites, Center for Translational Research in Neurodegenerative Disease, College of Medicine, University of Florida, 1275 Center Drive, BMS J-496, P.O. Box 100159, Gainesville, Florida 32610, USA. E-mail: levites.yona@ufl.edu*

© The American Society of Gene & Cell Therapy

although delivery into the cisterna magna (ICM) also results in moderate transduction of the spinal cord and brain. Intramuscular (IM) injection of rAAV2/8 or rAAV2/9 results in modest transduction of spinal motor and sensory neurons as well as limited transduction of CNS neurons. Notably, these robust transduction patterns were achieved by using $1–2\times10^{10}$ genomes, ~10–40 times less virus than what is typically used for intravenous or peripheral administration for targeting the spinal cord.[13–16] To illustrate the potential utility of this technique, we further show that expression of murine Interleukin (IL)-10 delivered by direct IS injection to neonatal SOD1-G93A mice that model familial Amyotrophic lateral sclerosis (ALS), prolongs survival and alters the inflammatory milieu of the spinal cord. Thus, we have established (i) optimal delivery paradigms for transduction of the rodent spinal cord with rAAV vectors and (ii) the potential utility of this technique for conducting preclinical target validation studies in mouse models of neurodegenerative diseases.

RESULTS

Effect of viral entry route on the overall spinal cord biodistribution of rAAV

We have previously shown that intracerebroventricular injection mediated CNS delivery of rAAV2/1, 2/5, 2/8, and 2/9 in neonatal mice results in robust CNS biodistribution and unique tropism.[12] Building on these data, we explored neuraxis transduction and tropism for these serotypes following IM, ICM, or IS delivery to neonatal mouse pups (**Figure 1a**,**b**,**c**,**d**). We injected rAAV2/1, 2/5, 2/8, and 2/9 (1×10^{10} genomes in 1 µl for ICM and IS single injections and 2×10^{10} genomes in 2 µl for bilateral IM injections) at the indicated injection site and aged the injected mice for 4 weeks. Direct EGFP fluorescence on excised spinal cords showed that the IS injection resulted in the highest level of transgene expression, irrespective of the capsid used (**Figure 1e**). Among the serotypes tested, rAAV2/1, rAAV2/5, and rAAV2/8 injected cohorts showed robust spinal cord EGFP expression (**Figure 1e**). In the ICM injected cohort, rAAV2/8

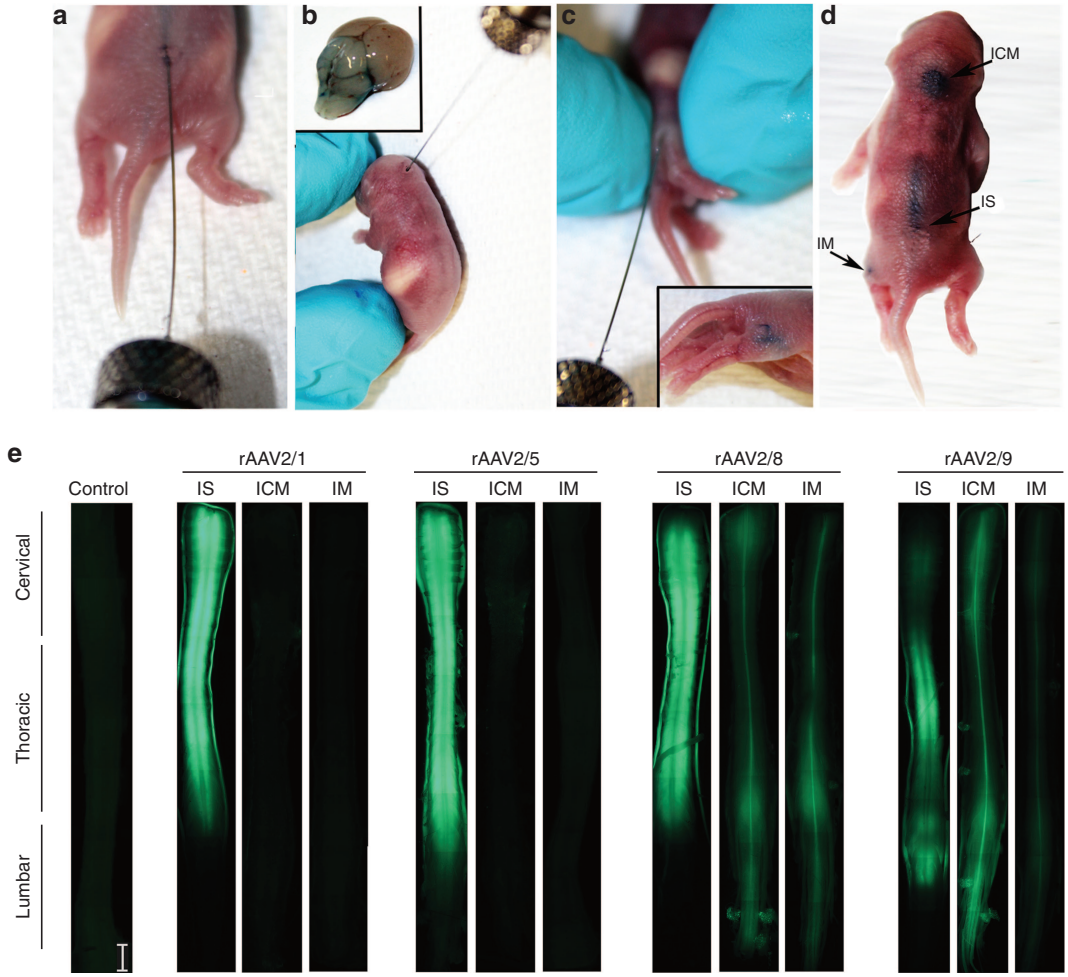

Figure 1 Demonstration of the three routes of rAAV injection used in this study. For the purpose of demonstration, 1 µl of 1% Evans blue dye was used followed by immediate visualization of the extent and localization of the blue dye. IS injection of 1 µl dye into the lumbar spinal cord ta a depth of 1–2 mm (**a**) resulted in coverage of the lower half of the spinal cord (**d**). ICM injection site is located under the skull and is best targeted when the pups head is bent forward (**b**,**d**). The brainstem and fourth ventricle are stained with the dye following injection of the dye into a depth of 1.5 mm (inset, **b**). For targeting the hindlimb muscle, IM injection was performed (**c**,**d**) at a depth of 3–5 mm, resulting in localized dye in the thigh region. (**e**) Representative fluorescence micrographs of formalin fixed entire spinal cords of uninjected mice (Control) or mice injected neonatally with rAAV2/1, 2/5, 2/8, or 2/9 expressing EGFP. IS injection of all serotypes resulted in robust and widespread expression of EGFP. ICM and IM injections of rAAV2/8 and rAAV2/9 displayed widespread EGFP expression, while injection of rAAV2/1 and rAAV2/5 via the ICM and IM routes showed either low levels of EGFP fluorescence or no detectable expression, respectively. Scale bar, 2 mm. n = 3–4/group. rAAV, recombinant adeno-associated virus; IS, lumbar spinal cord; ICM, cisterna magna; IM, intramuscular.

© The American Society of Gene & Cell Therapy

and rAAV2/9 produced higher levels of spinal cord transduction with limited transduction observed with rAAV2/1 or 2/5 (**Figure 1e**). IM injection of only rAAV2/8 and rAAV2/9 resulted in perceptible EGFP expression in the spinal cord (**Figure 1e**).

Cellular tropism and transduction patterns of rAAVs in the spinal cord following IM, ICM, or IS delivery

Paraffin embedded sections of the rAAV-injected spinal cords were stained with anti-EGFP antibody to enable quantification of total EGFP signal as well as offer further insight into the tropism of the various serotypes (**Figure 2**; **Supplementary Figures S1, S2, and S3; Supplementary Table S1**). Additionally, spinal cords were co-stained with anti-EGFP antibody (green fluorescent labeling) and antibodies to markers specific for each cell type (NeuN for neurons, ChAT for motor neurons, GFAP for astrocytes, red fluorescent labeling) (**Figure 3**). When total EGFP levels were quantified and compared in different groups, following pattern was revealed: For rAAV-IS injection 2/9 > 2/1 > 2/8 > 2/5, for ICM injection 2/9 > 2/8 > 2/1 > 2/5, for IM injection 2/8 > 2/9 >2/1 > 2/5. IS injection of rAAVs revealed interesting patterns, in terms of spread and tropism depending upon the serotype (**Figures 2** and **3**). All four serotypes resulted in robust transduction in the dorsal and ventral regions of the spinal cord, with EGFP expression evident in sensory and motor neurons and some astrocytes (**Figures 2** and **3**). The highest motoneuron transduction was seen in rAAV2/8 injected cohort with lowest levels in rAAV2/5 group (2/8 > 2/1 > 2/9 > 2/5). rAAV2/8 and 2/1 demonstrated high levels of EGFP expression in the cervical spinal cord, farthest from the site of injection. rAAV2/1 and 2/9 produced high levels of white

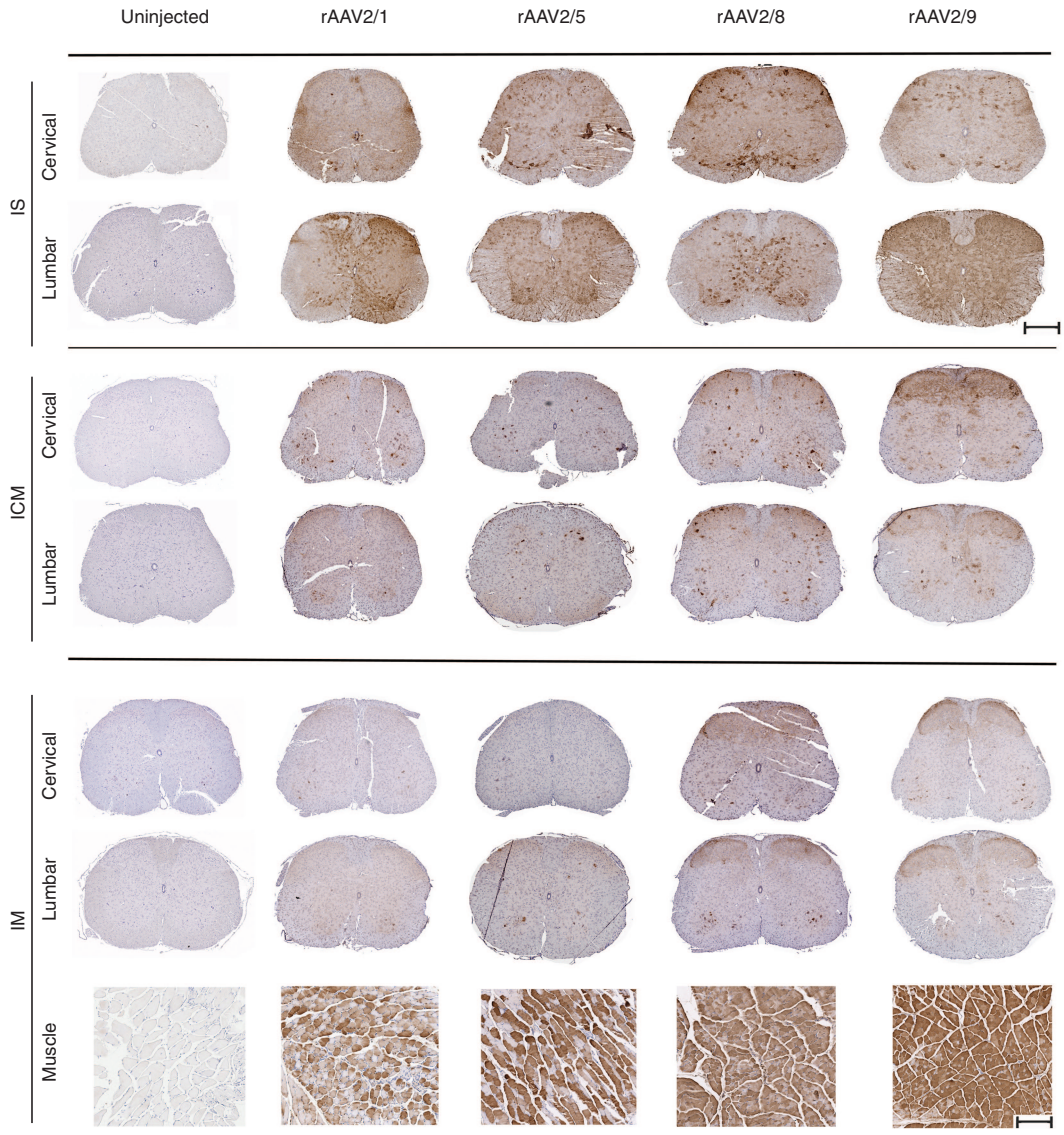

Figure 2 Comparative spinal cord biodistribution patterns of different rAAVs injected via IS, ICM, or IM routes. EGFP expression in cervical and lumbar spine in mice injected with rAAV-EGFP via IS, ICM, and IM routes on neonatal day P0. Uninjected tissue served as control. The 3-week old IS cohort showed EGFP expression spread throughout the spinal cord for all the serotypes tested. ICM injected cohorts show robust EGFP expression for rAAV2/8 and 2/9, but weak and infrequent expression for 2/5 or 2/1. All IM injected mice show widespread hindlimb muscle transduction and widespread but weak transgene expression in rAAV2/8 and rAAV2/9 injected spinal cords while no detectable EGFP expression was seen in either rAAV2/1 or rAAV2/5 injected spinal cords. Scale bar, 500 µm (Spinal cord), 200 µm (muscle). *n* = 3–4/group. rAAV, recombinant adeno-associated virus; IS, lumbar spinal cord; ICM, cisterna magna; IM, intramuscular.

© The American Society of Gene & Cell Therapy

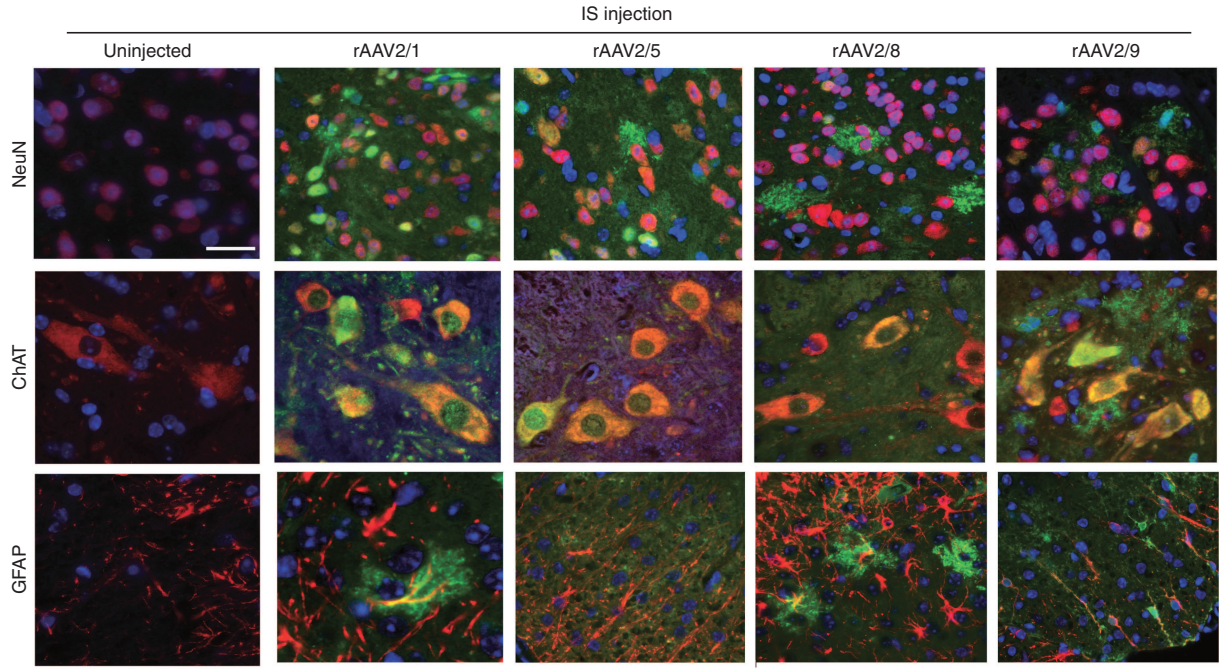

Figure 3 Comparative cellular tropism of spinal cord targeted rAAVs following IS delivery in neonatal mice. EGFP expression in the spinal cords of mice injected with different rAAV serotypes via IS route on neonatal day P0. Representative tricolor merged fluorescent photomicrograph from 3-week-old mice spinal cord sections were generated following co-labeling with anti EGFP antibody (488 nm—green), DAPI (350 nm—blue) and cell type specific marker antibodies (568 nm—red) for neurons (NeuN), motor neurons (ChAT), and astrocytes (GFAP). Scale bar, 50 µm. rAAV, recombinant adeno-associated virus; IS, lumbar spinal cord.

matter staining, with rAAV2/9 showing prominent oligodendrocytic and neuronal process transduction (**Figure 2**).

In the ICM group, all the serotypes demonstrated EGFP expression throughout the spinal cord, even sites distal to the site of entry such as the lumbar region (2/9 > 2/8 > 2/1 > 2/5). AAV2/1-EGFP was shown to be localized in the dorsal and ventral grey matter as well as neuropil and white matter (**Figure 2**). rAAV2/5-EGFP showed a similar pattern, albeit much weaker and was restricted to the ventral horn. On the other hand, both rAAV2/8 and 2/9 showed very robust spinal cord transduction, with EGFP present in neurons of both the dorsal and ventral horns, neuropil, and astrocytes (**Supplementary Figure S2**). EGFP expression in the dorsal horn, proximal to the site of injection, was especially prominent in the rAAV2/9 cohort.

In the IM cohort, all serotypes resulted in robust transduction of the hindlimb muscle with both rAAV2/1 and rAAV2/5 transducing a very limited number of cells in the spinal cord (**Figure 2**). By contrast, rAAV2/8 and 2/9 produced EGFP expression in scending sensory fibers, dorsal horn sensory neurons, motor neurons, and astrocytes (2/8 > 2/9) (**Figure 2**, **Supplementary Figure S3**).

Brain transduction of rAAVs following IM, ICM, or IS delivery

IS injection of rAAV2/8, 2/5, and 2/1 led to limited transduction of the motor cortex (2/8 > 2/5 > 2/1) (**Figure 4**) as well as brainstem (2/1 > 2/8 > 2/5) and retrosplenial cortical neurons (2/8 > 2/5 > 2/1) (**Supplementary Figure S4**). The most robust and widespread brain transduction in the IS cohort was observed in the rAAV2/9 mice, encompassing all the brain areas tested (**Supplementary Figure S4**). Not surprisingly, the ICM cohorts showed more significant brain transduction compared to the other entry routes (2/9 > 2/8 > 2/1 > 2/5) (**Supplementary Figure S5**). rAAV2/1 was transported to the retrosplenial cortex, possibly via the projections to the pons area, which is in close juxtaposition to the CM. rAAV2/5 showed very weak staining pattern in the brain, restricted to only caudal areas. The rAAV2/9 and 2/8 injected cohorts showed intense EGFP staining in all brain areas tested: strongest in the brainstem and cerebellum and spreading to distal areas including the retrosplenial cortex, cingulate cortex, dentate gyrus, hippocampal formation, and hypothalamus (**Figure 4**; **Supplementary Figure S5**). Both rAAV2/8 and 2/9 strikingly transduced the molecular layer of the dentate gyrus, whereas only rAAV2/8 robustly transduced the olfactory bulb neurons, possibly via lateral olfactory tract projections from the piriform cortex. In the IM injection group, examination of the brain showed very sporadic EGFP immunopositivity spread in the dentate gyrus, hippocampal CA4, Purkinje neurons, and choroid plexus in both rAAV2/8 and rAAV2/9 injected cohorts (**Supplementary Figure S6**). Neither rAAV2/1 or rAAV2/5 transduced the brain following IM delivery (**Figure 4**).

Dorsal root ganglia transduction by rAAVs following IM, ICM, or IS delivery

Optimizing transgene expression to the primary sensory neurons in the dorsal root ganglia may have critical implications for studies targeting peripheral nervous system disorders. We found that both rAAV2/8 and rAAV2/9 could robustly transduce the dorsal root ganglias, irrespective of the site of entry (**Supplementary Figure S7**). However, rAAV2/1 transduced dorsal root ganglia only in the IS cohort, whereas rAAV2/5 did not (**Supplementary Figure S7**).

© The American Society of Gene & Cell Therapy

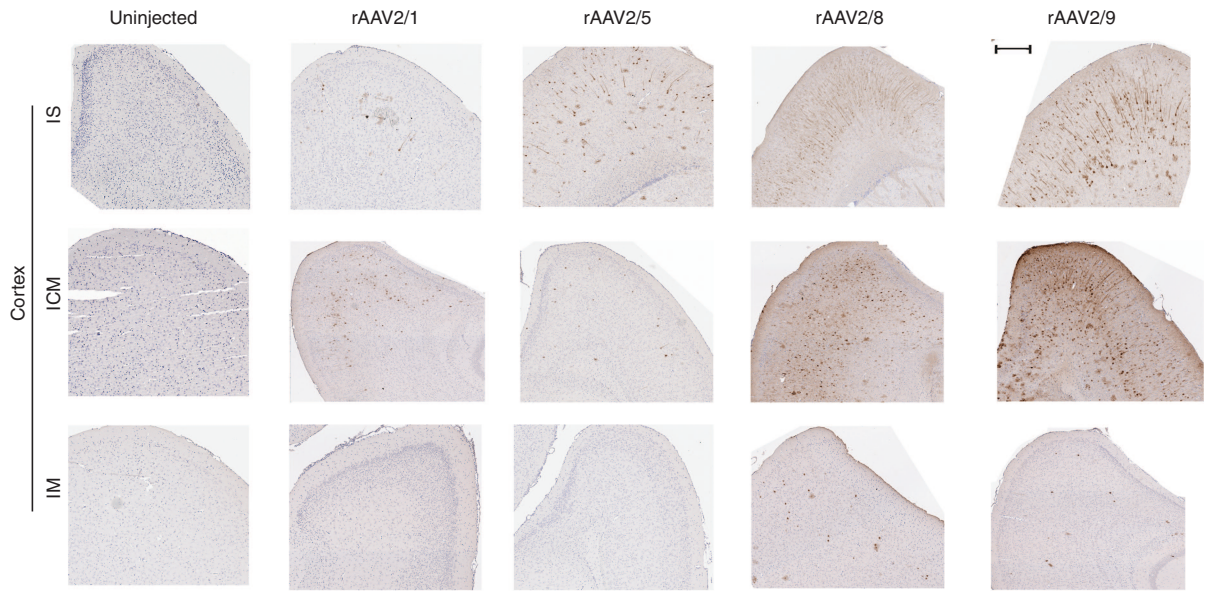

Figure 4 Differential transduction patterns of the frontal cortex by rAAVs delivered via IS, ICM, or IS routes. EGFP expression in the frontal cortex of mice injected with different rAAV serotypes via IS, ICM, or IM on neonatal day P0. Uninjected tissue served as control. Representative sections from 3-week-old mice show EGFP staining in the frontal cortex area of the brain. Scale bar, 500 µm. *n* = 3–4/group. rAAV, recombinant adeno-associated virus; IS, lumbar spinal cord; ICM, cisterna magna; IM, intramuscular.

IS delivery of rAAV2/1-IL-10 prolongs life expectancy in G93ASOD1 mouse model

Inflammatory responses are upregulated in the spinal cords of patients with ALS, a disease with progressive motoneuron degeneration, and in SOD1-G93A transgenic mice that recapitulate the clinicopathology of ALS. In general, the pro-inflammatory changes occur at sites of motoneuron injury early in the disease process, suggesting that dampening inflammation may potentially have a disease modifying effect.[17] To explore whether attenuating the inflammatory state could alter disease onset or progression in SOD1-G93A mouse, we delivered rAAV2/1-IL-10 via IS injection to newborn mice. This pilot was designed with a primary readout of survival (time to moribund state due to paralysis). Two control groups were established: an uninjected group and a group injected with rAAV2/1-EGFP. In non-transgenic littermates, IL-10 had no untoward effects within an observation period of 180 days (**Figure 5**). Further, IS injection of rAAV2/1-EGFP did not alter survival of the SOD1-G93A transgenic mice compared to the non-injected control transgenics (**Figure 5a**). Interestingly, rAAV2/1-IL-10 significantly increased survival when compared to the control group (↑15.2%, $P < 0.005$). Body weight (BW) analysis over time, however, showed no significant differences in the onset of weight loss in the rAAV2/1-IL-10 group, suggesting that IL-10 prolongs survival without changing onset (**Figure 5b**). At end stage, IL-10 was elevated in the spinal cords of AAV2/1-IL-10 injected mice (2.53 ± 3.12 ng/ml; 4.01× over control, $P = 0.036$). To establish expression levels of IL-10 in pre-symptomatic ages, IL-10 levels were assessed 3 weeks after the administration in the spinal cords of young SOD1 mice, confirming that rAAV-IL10 administration results in significant increase of IL-10 levels as compared to phosphate-buffered saline (PBS)-injected controls (**Figure 5c**). To assess the effect of IL-10 on astrocytosis and microgliosis, spinal cord tissues from paralyzed G93A mice and age-matched nontransgenic mice were immunostained with antibody to GFAP and Iba-1, respectively. As expected, the signal for both antibodies was significantly higher in the spinal cord of SOD1-G93A mice compared to controls, but neither antibody showed major changes in intensity when IL-10 was overexpressed. (**Figure 5d,e**). Analysis of spinal cord mRNA levels by Nanostring nCounter array revealed that IL-10 expression significantly reduced a subset of the innate immunity genes that were upregulated in end stage naive SOD1-G93A mice (**Figure 5f**; **Supplementary Table S2**). Among the attenuated genes in the spinal cords of end-stage SOD1-G93A mice expressing IL-10 were: various chemokines (Ccl3, Ccl11, Ccl4, and Cxcl10), Toll-like receptors (TLR1, 2, 6, and 7), complement pathway genes (c1qa, c1qb, c1r, c3ar1, c3, and cfd), and other factors (Hsbp1, Itgb2, and maff) (**Supplementary Table S2**). On the other hand, IL-10 also increased a subset of chemokines (Ccl5, Ccl8, and Cxcl9) and the co-stimulatory molecule cd40. IL-10 treatment also increased the transcription factor Stat1 but attenuated the expression of Myl2 (**Figure 5f**). Collectively, these data establish that over-expression of IL-10 produce an immune modulatory effect and these changes in inflammatory signaling correlate with longer survival in the SOD1-G93A model.

DISCUSSION

We sought to optimize rAAV-mediated gene targeting in the spinal cords of mice and used this information in a pilot study to assess the disease modifying potential of IL-10 in a well-studied mouse model of ALS. Our findings demonstrate the influence of capsid serotypes and route of virus entry on the biodistribution and transgene expression in mouse spinal cord and brain. We find that by far the most effective route of delivery resulting in rAAV transduction of the entire spinal cord is direct lumbar injection in neonatal mice. Using direct IS injection, rAAV2/1, 5, 8, and 9 result in robust expression of the EGFP transgene throughout

© The American Society of Gene & Cell Therapy

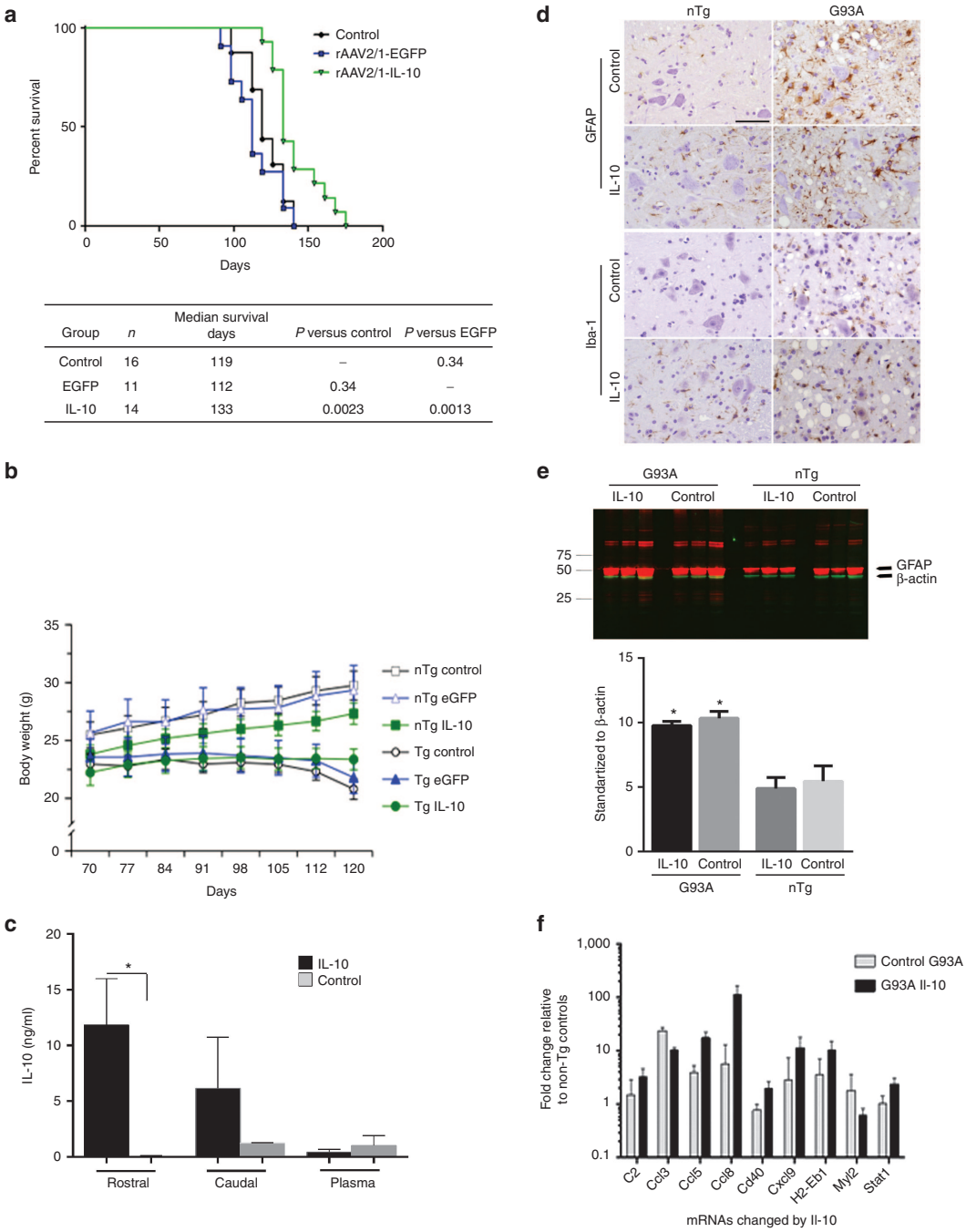

Group	*n*	Median survival days	*P* versus control	*P* versus EGFP
Control	16	119	–	0.34
EGFP	11	112	0.34	–
IL-10	14	133	0.0023	0.0013

Figure 5 Extension of life span in rAAV2/1-IL-10 injected SOD1G93A mice. (**a**) IS administration of rAAV2/1-IL-10 in neonatal mice increases life span of SOD1G93A mice without affecting disease onset. Kaplan–Meier curve for survival shows that IL-10 expression extends the life span by 15.2% over the control group. No difference in median survival was noted between the rAAV2/1-EGFP injected mice and control (uninjected) mice. (**b**) IL-10 injected SOD1G93A mice maintained their body weights as compared to age-matched controls during their prolonged survival. Body weights of mice are graphically presented from day 70 postnatal till day 160, when the entire control group succumbed to paralysis. IL-10 expression did not significantly changed the body weight of non-Tg mice; however, the IL-10 injected SOD1G93A mice showed consistent trend of lower weight compared to controls ($P = 0.1$). $n = 12, 7, 22$ for uninjected, rAAV2/1-EGFP, and rAAV2/1-IL-10 nontransgenic cohort; $n = 16, 7, 14$ for uninjected, rAAV2/1-EGFP, and rAAV2/1-IL-10 SOD1G93A cohort. (**c**) IL-10 levels were quantified by ELISA of soluble spinal cord lysates from the rostral and caudal parts from 3 weeks old SOD1 G93A mice injected with rAAV-IL-10 on neonatal day P0. $n = 5$–10 mice, $P < 0.05$, *t*-test. (**d**) GFAP and Iba-1 immunohistochemistry showed increased immunoreactivity in the spinal cords of end-stage SOD1G93A (G93A±) mice as compared to age-matched nontransgenic (NTg) controls. IL-10 overexpression did not significantly modify this pathology. $n = 5$/group. (**e**) Representative anti-GFAP immunoblot and intensity analysis of immunoreactive GFAP protein levels (mean ± SEM), normalized to β-actin showing that SOD1 mice have elevated levels of GFAP as compared to controls. There were no significant changes in GFAP levels in mice overexpressing IL-10 compared to genotype-matched controls ($n = 3$/group; $P > 0.05$, *t*-test). (**f**) Nanostring RNA profiling of spinal cords from nontransgenic and SOD1G93A mice showed that multiple immune mediators were affected in response to IL-10. A representative set of immune genes that were most significantly affected are depicted here after adjusting for a false discovery rate of 0.1%. For the complete array data, please see **Supplementary Table S2**. $n = 3$–4/group; $P < 0.001$, 1 way Anova. rAAV, recombinant adeno-associated virus; IS, lumbar spinal cord; IL, interleukin.

© The American Society of Gene & Cell Therapy

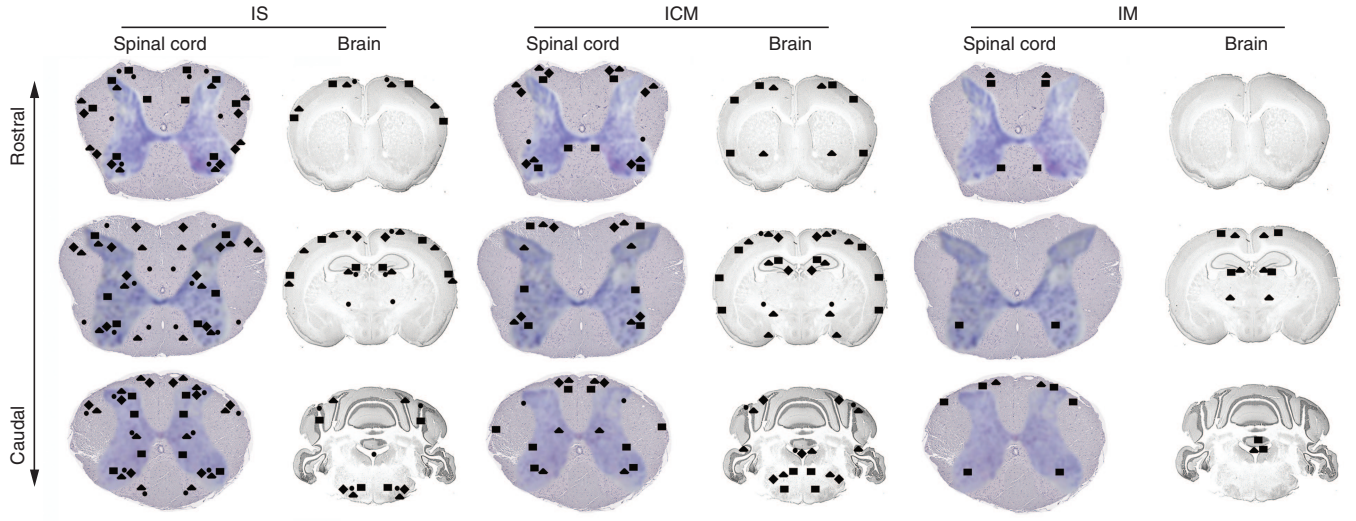

Figure 6 Schematic depiction of rAAV transduction in the brain and spinal cord following IM, ICM, and IS injection. Data based on EGFP expression patterns from this study has been summarized to depict the relative biodistribution properties of different rAAV serotypes transduced via IM, ICM, and IS injection routes. (diamond symbol) rAAV2/1; (filled circle) rAAV2/5; (squate symbol) rAAV2/8; (triangle symbol) rAAV2/9. Please see **Table 1** for details. rAAV, recombinant adeno-associated virus; IS, lumbar spinal cord; ICM, cisterna magna; IM, intramuscular.

the spinal cord. rAAV serotypes 1 and 9 appear to transduce the broadest spectrum of cell types with serotype 8 showing a marked neurotropism. ICM delivery of rAAV2/8 or 2/9 results in transduction of both brain and spinal cord, but the level of expression in the caudal cord was markedly lower than what was achieved by IS injection. Delivery of rAAV with capsid serotypes 8 and 9 by IM injection produced a more limited expression that appeared to be largely neuronal. Notably, all of the rAAV serotypes efficiently transduced the vast majority of muscle fibers in the injected limb following IM injection.

Building on these observations, we tested whether effect of IS delivered rAAV2/1 encoding IL-10 would produce immune modulation in in the SOD1-G93A mouse model. We found that we could achieve significant increases in the level of spinal cord IL-10 protein and that lifelong expression of IL-10 resulted in altered expression levels of a number of genes involved in innate immunity, indicating that over-expression of IL-10 modified the local immune milieu. These changes in inflammatory signaling were accompanied by prolonged survival of the G93A mice. In particular, changes in the expression of numerous chemokine genes were associated with increased survival (Ccl5 and Ccl8), suggesting that recruitment and activation of peripheral or spinal cord resident myeloid cells can have a potential beneficial effect.

We observed that we could manipulate cell tropism and regional patterns of transgene expression by varying the capsid serotype and viral entry route (**Figure 6**, **Table 1**). For example, though overall transduction of the spinal cord following IS delivery was fairly similar, there were clear differences in cell tropism. rAAV2/9 showed the most robust neurotropism, including motor neurons. There was strong expression of EGFP in sensory afferents in mice injected IS with rAAV2/9-EGFP. rAAV2/5 and 2/8 were broadly expressed, but showed strong preference for neurons in general while rAAV2/1 expressed in both neurons and astrocytes. These data somewhat contrast our previous observations in which these same rAAV2/1 viruses encoding EGFP were injected into the cerebral ventricles of newborn mice and found to be neurotropic while rAAV5 selectively targeted astrocytes.[12] Thus, when used in neonatal injection it may be possible to target specific populations of spinal neural cells by modulating rAAV capsid serotype and route of viral entry.

The mechanism by which rAAV is transported to the spinal cord and the brain following peripheral injection is yet to be determined. Based on previous observations, it is likely that motor and sensory neurons in the spinal cord and brain can be transduced by either of two processes: retrograde transport of the rAAV directly through neuromuscular junctions or uptake across the blood–brain barrier.[13] Our data strongly support a retrograde transport mechanism. The rAAV vectors with capsids 8 and 9 that were injected into muscle transduced the muscle, dorsal root ganglion, spinal cord, and scattered neurons in the cortex, the latter consistent with upper motor and sensory neurons. We also found little evidence that the rAAV enters the systemic circulation or transduces peripheral organs, suggesting that direct trans-synaptic transport mediated the selective pattern of transduction along motor and sensory pathways (data not shown).

Several studies have demonstrated the efficacy of rAAV directed therapeutic approaches using intramuscular, intravenous, intraperitoneal, intrathecal, or intra-nerve administration in rodent models of lower MNDs (*e.g.*, ALS and spinal muscular atrophy), spinal cord injury, peripheral pain, or other degenerative diseases (motor and sensory neuropathies, spinocerebellar ataxias, and Huntington's disease) (reviewed in "ref. 18"). Many of these reports have observed cell type specific transduction of spinal cord targeted rAAVs: for example, rAAV9 preferentially transduces astrocytes or oligodendrocytes and rAAV1 targets lower motor neurons in adult animals.[19–21] However, we did not notice any exclusive cell type selectivity of the different capsids, in concordance to other reports.[14,22] Such peripheral to central gene therapy paradigms have also been reproduced successfully in larger animals, including non-human primates. IM injection of AAV6 and intrathecal injection of AAV9, and AAV7, have been shown to result in modest but efficient transduction of non-human primate

© The American Society of Gene & Cell Therapy

Table 1 Comparative summary of the spinal cord transduction characteristics of different rAAV serotypes following IS, ICM, and IM delivery

	IS	ICM	IM
Neurons	2/1, 2/5, 2/8,2/9	2/1, 2/5, 2/8,2/9	2/8
Motor neurons	2/1, 2/5, 2/8,2/9	—	—
Neuronal processes	2/1, 2/5, 2/8, 2/9	2/9	2/8
Astrocytes	2/1, 2/5, 2/8, 2/9	2/8, 2/9	2/8, 2/9
Microglia	—	—	—
Dorsal WM	2/1, 2/8, 2/9	2/8, 2/9	2/8, 2/9
Dorsal GM	2/1, 2/5, 2/8, 2/9	2/5, 2/8, 2/9	—
Ventral WM	2/1, 2/8, 2/9	—	—
Ventral GM	2/1,2/5, 2/8, 2/9	2/1, 2/5, 2/8, 2/9	2/8, 2/9
DRG	2/1, 2/8, 2/9	2/8, 2/9	2/8, 2/9

WM, white matter; GM, grey matter; DRG, dorsal root ganglia; IS, lumbar spinal cord; ICM, cisterna magna; IM, intramuscular.
Please see **Figure 6** for graphical representation.

spinal cords without substantial immune response, establishing a clear precedence for the translatability of our preclinical paradigms to large animal models of MNDs.[23–26] It appears that a direct spinal cord administration (IS or ICM) facilitates in maintaining neuraxis transgene expression even in the presence of peripherally circulating anti-AAV-neutralizing antibodies.[27] One caveat of the early studies on spinal cord targeting of rodents using peripheral entry sites was that the AAV transduction was mostly proximal to the site of entry and required multiple injections of high genome particles along the neuraxis for efficient transduction.[28] Here, we have demonstrated the efficacy of a single IS bolus of rAAV2/8 and rAAV2/9 in yielding unprecedented high levels of EGFP expression throughout the neuraxis, even extending to the olfactory bulb in the brain. Indeed, viruses of serotypes 8 and 9 were effective in transducing a large fraction of both upper and lower motor neurons, relevant for therapeutic targeting of a host of neuromuscular diseases.

Although rAAV could be used to deliver therapeutic biologics that act cell autonomously, the strategy is well suited to express proteins that are secreted and could affect homeostasis in a non-cell autonomous manner. We have previously demonstrated that various secreted immune modulators, expressed from rAAV vectors, can alter Aβ pathology *in vivo*.[7,29–32] There are complex changes in the inflammatory milieu of the spinal cord and peripheral immune system of SOD1 mouse models and human ALS patients. These include alterations in numerous chemokines, cytokines, and acute phase reactants, including down-regulation of IL-10, preceding disease onset.[33–35] It is becoming increasingly clear that the dynamic cross-talk between inflammatory signaling and ALS proteinopathy is a deterministic factor for disease progression following onset of symptoms.[33] A recent study has conclusively shown that reducing a subset of inflammatory monocytes ameliorated murine ALS.[35] Similarly, infiltration of regulatory T cells that display a predominantly anti-inflammatory phenotype dramatically delays ALS disease progression via induction of IL-4, IL-10, and TGFβ signaling.[34,36] Given these lines of evidence, we overexpressed IL-10, a master regulatory anti-inflammatory cytokine, which down-regulates the expression of pro-inflammatory cytokines, MHC class II antigens and co-stimulatory molecules on macrophages and monocytes. Our observations that IL-10 slows disease progression in SOD1-G93A mice without significantly affecting disease onset recapitulates observations from other groups involving transplanting wild type microglia or selective microglial excision of mutant SOD1 (using cre-lox technology) in ALS mice.[37,38] Given the current understanding of the non-cell autonomous nature of ALS, it is certainly challenging to infer whether the outcome in IL-10 treated mice is mechanistically driven solely by or as a combinatorial effect of altered innate immune milieu, including increased chemokine signaling, and mitigated proteinopathy. Nevertheless, the ability of rAAV directed IL-10 to modulate the inflammatory milieu toward a beneficial state provides us with a novel proof of concept to similarly manipulate inflammatory responses in other neurodegenerative or neuromuscular diseases. Given the safety and tolerability of IL-10 in clinical trials, our study reinforces its potential utility as a new line of therapeutic in ALS and other MNDs.[39]

In the context of MNDs, several challenges exist when translating preclinical proof of concept studies to clinical paradigms. Some of these confounding factors are low bioavailability, as target cells are widely distributed along the neuraxis; local toxicity due to high dose-exposure of transduced cells at point of entry and non-cell autonomous etiology of many of these diseases.[37,40,41] Efficacious therapy in ALS and other MNDs remains challenging, as any drug delivery strategies must ensure optimal bioavailability throughout the spinal cord, which ideally requires diffuse gene delivery along the entire neuraxis. In contrast, non-cell autonomous targeted paradigms can potentially overcome these challenges by ensuring broader spread of the transgene along the spinal cord and affecting the homeoostasis of multiple cell types simultaneously. Additionally, absence of systemic spread of the transgene in IS or ICM paradigms[27] makes this an attractive choice for reducing peripheral toxicity while maintaining high transgene levels in the spinal cord. Overall, our data demonstrate the feasibility of rAAV2/1, rAAV2/8, and rAAV2/9 in newborn animals as robust gene delivery vehicles to the entire spinal cord and selective areas of the CNS for preclinical modeling and testing preventative therapeutic strategies in MNDs. Our data also indicate that it should be possible to direct expression of genes in certain cell types by varying the rAAV serotype and route, and perhaps age, of delivery. Genes expressed from rAAV2/8 vectors should be more selectively expressed in motor neurons, whereas genes expressed from rAAV2/1 and rAAV2/9 should be expressed in all cell types, enabling non-cell autonomous paradigms of disease modification.

MATERIALS AND METHODS

AAV construction and preparation. AAV was prepared by methods described earlier.[42] Briefly, AAV vectors expressing the EGFP under the control of the cytomegalovirus enhancer/chicken beta actin promoter, a woodchuck hepatitis virus post-transcriptional-regulatory element, and the bovine growth hormone polyA (pAAV-EGFP) were generated by Polyethylenimine (PEI, Polysciences, Warrington, PA) transfection into HEK293T cell line. Cells were co-transfected with the AAV helper plasmids pDP1rs, pDP5rs, pDP8.ape, and pDG9. Helper Plasmid 1, 5, & 8 were obtained from Plasmid Factory, Germany. AAV9 (pDG9) was constructed

© The American Society of Gene & Cell Therapy

by isolating the backbone from the AAV helper plasmid pDG and the AAV9 capsid gene from pAAV 9 (S. Zolotukhin UF, Gainesville, FL). At 72 hours after transfection, cells were harvested and lysed in the presence of 0.5% Sodium Deoxycholate and 50 U/ml Benzonase (Sigma) by repeated rounds of freeze/thaws at −80 °C and 50 °C. The virus was isolated using a discontinuous Iodixanol gradient. Samples were buffer exchanged to PBS using an Amicon Ultra filter 100,000 MWCO Centrifugation device (EMD Millipore, Billerica, MA). The genomic titer of each virus was determined by quantitative PCR (Bio-Rad CFX384). The viral DNA samples were prepared by treating the virus with DNaseI (Life Technologies, Grand Island, NY), heat inactivating the enzyme, digesting the protein coat with Proteinase K (Life Technologies), and concluding with a second heat-inactivation. Samples were compared against a standard curve of supercoiled plasmid diluted to 1e3 to 1e7 copies per ml. Freshly prepared AAVs were aliquoted and stored at −80 °C. When needed, viruses were diluted in sterile 1X DPBS, pH7.2 and used immediately.

Mice and neonatal injections. All animal husbandry procedures performed were approved by University of Florida Institutional Animal Care and Use Committee (IACUC) in accordance with NIH guidelines. B6C3 mice were generated in our facility. Mice transgenic for G93A SOD1 were generated by breeding male hemizygous carriers (G6SJL-Tg(SOD1-G93A)1Gur/J) obtained from the Jackson Laboratories (Bar Harbor, ME) to female B6SJLF1 hybrids. All animals were housed three to five to a cage and maintained on *ad libitum* food and water with a 12 hours light/dark cycle.

Neonatal pups were injected within 0–6 hours after birth. The naive pups were covered in aluminum foil and completely surrounded in ice for 3–4 minutes, resulting in the body temperature being lowered to <10 °C. The pups are considered completely cryoanesthetized when all movement stops and the skin color changes from pink to purple. Cryoanesthetized neonates were injected using 10 µl syringes (1 inch needle, 30 degrees bevel; Hamilton Company, Reno, NV) via either IM, ICM, or IM as demonstrated in **Figure 1**. For IM injection, 2 µl of virus was injected into each of the caudal thigh muscles. For ICM injection, 1 µl of virus was injected directly into the spot on the neck below the skull and for IS delivery. 1 µl of virus was slowly injected into the spinal cord, which can be seen as a white line down their back, at 5 mm from the base of the tail. The injection starts almost parallel to the back when the needle punctures the skin, then the needle angle is increased to 50–60° to insert the needle into the vertebral column. After injection pups were allowed to completely recover on a warming blanket and then returned to the home cage.

RNA isolation and analysis. Total RNA from mouse spinal cords was purified using Trizol and RNaqueous kit (Ambion) and reverse transcribed using Superscript III (Invitrogen). Multiplex analysis of transcriptome was done using nCounter® GX mouse inflammation kit (NanoString Technologies, Seattle, WA) using 100 ng of total RNA from mice brains using manufacturer's recommendation.[43] This pre-built array consists of 179 inflammation-related genes and six internal reference genes. A list of the actual target genes is available at www.nanostring.com

Cytokine ELISA and GFAP immunoblotting. Neonatally injected spinal cords were used for protein extraction in the presence of RIPA buffer. Cytokine levels were analyzed from 1:10 diluted RIPA extracted lysates using BD OptiEIA ELISA kits. RIPA extracts were separated on Bis-Tris criterion XT gels (Bio-Rad, Hercules, CA) were probed with the antibody against glial fibrillary acidic protein (GFAP; 1:1000; DAKO, Carpinteria, CA) and anti-β-actin (1:1000; Sigma, St. Louis, MO). Relative band intensity was quantified using ImageJ software (National Institutes of Health, Bethesda, MD).

Immunohistochemical staining, imaging, and image processing. Brains, muscle and spinal cords were harvested following trans-cardial perfusion with PBS (Fisher Scientific, Waltham, MA). Dissected tissues were immersion fixed overnight in formalin solution at 4 °C. Prior to paraffin embedding, spinal cords were cut into 1-cm sections and brains were sagittal dissected. All tissues were embedded in paraffin and cut to a thickness of 5 µm and attached to glass slides (Fisher Scientific). Brains were cut sagittally while both longitudinal and cross-sections of muscles were collected. Immunohistochemistry was performed using an EGFP antibody (Invitrogen; 1:1000) followed by development using ImmPress polymer detection reagents (Vector Labs, Burlingame, CA). Immunohistochemically stained sections were captured using the Scanscope XT image scanner (Aperio Scanner; Leica Biosystems, Buffalo Grove, IL). Intensity of EGFP staining was calculated using the Positive Pixel Count program (Aperio). At least three sections per sample, 30µm apart, were averaged by a blinded observer. Double immunofluorescent staining was done using, NeuN (Cell Signaling, 1:100), Chat (Cell Signaling, 1:500), GFAP-Cy3 (Sigma, 1:1000), EGFP (JL-8, Clontech; 1:1000) or EGFP (Invitrogen; 1:1000) and developed using Alexa Fluor labeled secondary antibodies (1:500, Invitrogen). Fluorescently labeled sections were visualized on a Olympus BX60 microscope with a color camera. Brightness and contrast alterations were applied identically on captured images using Photoshop CS5.

In vivo EGFP fluorescence was detected by EVOS® FL Cell Imaging System (Life Technologies). Fixed spinal cords were placed on the preparation slide and series of longitudinal images were acquired at 4× magnification. For optimizing background fluorescence and inherent tissue fluorescence, non-injected cord was included. All the images were acquired at the same exposure. The images were stacked and stitched together using imaging software (Image J).

Body weight (BW) analysis and statistics. The initial sample sizes of mice in the experiment were 17 (9♂, 8♀), 7 (3♂, 4♀), 22 (9♂, 13♀) for the control (non-injected), EGFP and IL-10 injected non-Tg mice respectively, and 16 (5♂, 11♀), 7 (2♂, 5♀), and 14 (4♂, 10♀) for respective cohorts of Tg mice. The BW was recorded between 10 and 23 weeks (70 and ~160 days, respectively) of mice age. Since the inspection of the raw data revealed that from week 17 onwards Tg mice showed increased mortality, the analysis of changes in BW (repeated measure ANOVA) was performed on BW data from week 10 to 17 in order to run the analysis of intact sample sizes and thus retain the maximum power of statistical analysis. In addition, since preliminary analyses revealed that males were heavier than females in non-Tg and Tg cohorts (data not shown), the group sex composition was not balanced, especially in IL-10 injected Tg group which was female biased, therefore the treatment effects were analyzed with sex used as covariate which provided a statistical control of the effect of sex on BW.

The statistical analysis was performed by a factorial analysis of variance (ANOVA) with genotype (non-Tg and Tg), treatment (control (no-injection), EGFP, and IL-10 injection) and sex as between, and the age of body weight change (week 10 to week 17), as within subject (repeated measure) factors. A departure from the assumption of compound sphericity was evaluated by Mauchly sphericity test with α level set to 0.05. In cases when sphericity was violated, degrees of freedom were adjusted by Greenhouse-Geisser ε-correction. When appropriate, global factorial analysis was followed by analyses of simple effects pertaining to each research hypothesis. In analyses requiring multiple comparisons among means Bonferroni adjustment of α level to minimize Type 1 (family-wise) error rate was used. Post-hoc analyses were performed using Bonferroni *t* test (MODLSD). All statistical analyses were done using Statistical Package for Social Sciences (SPSS, Chicago) version 21 for Macintosh. Due to space limitation and considerable number of between- and within-subject factors only significant results pertaining directly to tested hypotheses are reported.

SUPPLEMENTARY MATERIAL

Figure S1. EGFP immunostaining (presented as % area) of each cohort was quantified by averaging the positive pixel count output (Aperio) from three slides spaced 30 µm apart, each containing two consecutive sections.

Figure S2. Cellular tropism in the spinal cord following ICM delivery of rAAVs in neonatal mice.

© The American Society of Gene & Cell Therapy

Figure S3. Cellular tropism in the spinal cord following IM delivery of rAAVs in neonatal mice.
Figure S4. EGFP expression mice brains injected IS with rAAV-EGFP on neonatal day P0.
Figure S5. EGFP expression in mice brains injected ICM with rAAV-EGFP on neonatal day P0.
Figure S6. EGFP expression in mice brains injected with rAAV-EGFP in hindlimb muscle on neonatal day P0.
Figure S7. EGFP expression in the DRG of mice injected with different rAAV serotypes via IM, ICM or IS routes on neonatal day P0.
Table S1. Overall tissue biodistribution properties of different rAAV serotypes delivered via IS, ICM or IM routes.
Table S2. Quantitative nCounter expression profiling of inflammatory mediators from spinal cords of SOD1G93A and nontransgenic mice.

ACKNOWLEDGMENT

Generous support from ALSA (TEG), the Ellison Medical Foundation, NIH AG018454 (TEG), the Wilder Family Fellowship and BrightFocus Foundation (PC) and gifts from The Prentice Foundation and the Babicka Family (YL).

T.E.G., D.B., Y.L., P.C., and J.I.A. conceptualized these studies. Y.L., P.C., and J.I.A. designed and conducted the experiments; P.C., Y.L., D.R.B., and T.E.G. wrote manuscript; Y.L., P.C., J.I.A., S.F., O.S., Z.S., A.L., K.W.C., and C.J. contributed to animal and histological experiments; P.E.C., A.W.M., and C.C.-D. prepared rAAV.

REFERENCES

1. Golde, TE, Borchelt, DR, Giasson, BI and Lewis, J (2013). Thinking laterally about neurodegenerative proteinopathies. *J Clin Invest* **123**: 1847–1855.
2. Cederfjäll, E, Nilsson, N, Sahin, G, Chu, Y, Nikitidou, E, Björklund, T *et al.* (2013). Continuous DOPA synthesis from a single AAV: dosing and efficacy in models of Parkinson's disease. *Sci Rep* **3**: 2157.
3. Murphy, SR, Chang, CC, Dogbevia, G, Bryleva, EY, Bowen, Z, Hasan, MT *et al.* (2013). Acat1 knockdown gene therapy decreases amyloid-β in a mouse model of Alzheimer's disease. *Mol Ther* **21**: 1497–1506.
4. Furman, JL, Sama, DM, Gant, JC, Beckett, TL, Murphy, MP, Bachstetter, AD *et al.* (2012). Targeting astrocytes ameliorates neurologic changes in a mouse model of Alzheimer's disease. *J Neurosci* **32**: 16129–16140.
5. Bu, J, Ashe, KM, Bringas, J, Marshall, J, Dodge, JC, Cabrera-Salazar, MA *et al.* (2012). Merits of combination cortical, subcortical, and cerebellar injections for the treatment of Niemann-Pick disease type A. *Mol Ther* **20**: 1893–1901.
6. Cearley, CN, Vandenberghe, LH, Parente, MK, Carnish, ER, Wilson, JM and Wolfe, JH (2008). Expanded repertoire of AAV vector serotypes mediate unique patterns of transduction in mouse brain. *Mol Ther* **16**: 1710–1718.
7. Chakrabarty, P, Ceballos-Diaz, C, Beccard, A, Janus, C, Dickson, D, Golde, TE *et al.* (2010). IFN-gamma promotes complement expression and attenuates amyloid plaque deposition in amyloid beta precursor protein transgenic mice. *J Immunol* **184**: 5333–5343.
8. Levites, Y, Jansen, K, Smithson, LA, Dakin, R, Holloway, VM, Das, P *et al.* (2006). Intracranial adeno-associated virus-mediated delivery of anti-pan amyloid beta, amyloid beta40, and amyloid beta42 single-chain variable fragments attenuates plaque pathology in amyloid precursor protein mice. *J Neurosci* **26**: 11923–11928.
9. Mandel, RJ, Manfredsson, FP, Foust, KD, Rising, A, Reimsnider, S, Nash, K *et al.* (2006). Recombinant adeno-associated viral vectors as therapeutic agents to treat neurological disorders. *Mol Ther* **13**: 463–483.
10. Mingozzi, F and High, KA (2011). Therapeutic *in vivo* gene transfer for genetic disease using AAV: progress and challenges. *Nat Rev Genet* **12**: 341–355.
11. Asokan, A, Schaffer, DV and Samulski, RJ (2012). The AAV vector toolkit: poised at the clinical crossroads. *Mol Ther* **20**: 699–708.
12. Chakrabarty, P, Rosario, A, Cruz, P, Siemienski, Z, Ceballos-Diaz, C, Crosby, K *et al.* (2013). Capsid serotype and timing of injection determines AAV transduction in the neonatal mice brain. *PLoS One* **8**: e67680.
13. Foust, KD, Nurre, E, Montgomery, CL, Hernandez, A, Chan, CM and Kaspar, BK (2009). Intravascular AAV9 preferentially targets neonatal neurons and adult astrocytes. *Nat Biotechnol* **27**: 59–65.
14. Benkhelifa-Ziyyat, S, Besse, A, Roda, M, Duque, S, Astord, S, Carcenac, R *et al.* (2013). Intramuscular scAAV9-SMN injection mediates widespread gene delivery to the spinal cord and decreases disease severity in SMA mice. *Mol Ther* **21**: 282–290.
15. Klaw, MC, Xu, C and Tom, VJ (2013). Intraspinal AAV injections immediately rostral to a thoracic spinal cord injury site efficiently transduces neurons in spinal cord and brain. *Mol Ther Nucleic Acids* **2**: e108.
16. Kaspar, BK, Lladó, J, Sherkat, N, Rothstein, JD and Gage, FH (2003). Retrograde viral delivery of IGF-1 prolongs survival in a mouse ALS model. *Science* **301**: 839–842.
17. Henkel, JS, Beers, DR, Zhao, W and Appel, SH (2009). Microglia in ALS: the good, the bad, and the resting. *J Neuroimmune Pharmacol* **4**: 389–398.
18. Dayton, RD, Wang, DB and Klein, RL (2012). The advent of AAV9 expands applications for brain and spinal cord gene delivery. *Expert Opin Biol Ther* **12**: 757–766.
19. Foust, KD, Wang, X, McGovern, VL, Braun, L, Bevan, AK, Haidet, AM *et al.* (2010). Rescue of the spinal muscular atrophy phenotype in a mouse model by early postnatal delivery of SMN. *Nat Biotechnol* **28**: 271–274.
20. Hollis, ER 2nd, Kadoya, K, Hirsch, M, Samulski, RJ and Tuszynski, MH (2008). Efficient retrograde neuronal transduction utilizing self-complementary AAV1. *Mol Ther* **16**: 296–301.
21. Bucher, T, Colle, MA, Wakeling, E, Dubreil, L, Fyfe, J, Briot-Nivard, D *et al.* (2013). scAAV9 intracisternal delivery results in efficient gene transfer to the central nervous system of a feline model of motor neuron disease. *Hum Gene Ther* **24**: 670–682.
22. Zheng, C, Voutetakis, A, Metzger, M, Afione, S, Cotrim, AP, Eckhaus, MA *et al.* (2010). Evaluation of a rapamycin-regulated serotype 2 adeno-associated viral vector in macaque parotid glands. *Oral Dis* **16**: 269–277.
23. Towne, C, Setola, V, Schneider, BL and Aebischer, P (2011). Neuroprotection by gene therapy targeting mutant SOD1 in individual pools of motor neurons does not translate into therapeutic benefit in fALS mice. *Mol Ther* **19**: 274–283.
24. Passini, MA, Bu, J, Richards, AM, Treleaven, CM, Sullivan, JA, O'Riordan, CR *et al.* (2014). Translational fidelity of intrathecal delivery of self-complementary AAV9-survival motor neuron 1 for spinal muscular atrophy. *Hum Gene Ther* **25**: 619–630.
25. Foust, KD, Salazar, DL, Likhite, S, Ferraiuolo, L, Ditsworth, D, Ilieva, H *et al.* (2013). Therapeutic AAV9-mediated suppression of mutant SOD1 slows disease progression and extends survival in models of inherited ALS. *Mol Ther* **21**: 2148–2159.
26. Samaranch, L, San Sebastian, W, Kells, AP, Salegio, EA, Heller, G, Bringas, JR *et al.* (2014). AAV9-mediated expression of a non-self protein in nonhuman primate central nervous system triggers widespread neuroinflammation driven by antigen-presenting cell transduction. *Mol Ther* **22**: 329–337.
27. Gray, SJ, Nagabhushan Kalburgi, S, McCown, TJ and Jude Samulski, R (2013). Global CNS gene delivery and evasion of anti-AAV-neutralizing antibodies by intrathecal AAV administration in non-human primates. *Gene Ther* **20**: 450–459.
28. Snyder, BR, Gray, SJ, Quach, ET, Huang, JW, Leung, CH, Samulski, RJ *et al.* (2011). Comparison of adeno-associated viral vector serotypes for spinal cord and motor neuron gene delivery. *Hum Gene Ther* **22**: 1129–1135.
29. Chakrabarty, P, Ceballos-Diaz, C, Lin, WL, Beccard, A, Jansen-West, K, McFarland, NR *et al.* (2011). Interferon-γ induces progressive nigrostriatal degeneration and basal ganglia calcification. *Nat Neurosci* **14**: 694–696.
30. Chakrabarty, P, Jansen-West, K, Beccard, A, Ceballos-Diaz, C, Levites, Y, Verbeeck, C *et al.* (2010). Massive gliosis induced by interleukin-6 suppresses Abeta deposition in vivo: evidence against inflammation as a driving force for amyloid deposition. *FASEB J* **24**: 548–559.
31. Chakrabarty, P, Tianbai, L, Herring, A, Ceballos-Diaz, C, Das, P and Golde, TE (2012). Hippocampal expression of murine IL-4 results in exacerbation of amyloid deposition. *Mol Neurodegener* **7**: 36.
32. Chakrabarty, P, Herring, A, Ceballos-Diaz, C, Das, P and Golde, TE (2011). Hippocampal expression of murine TNFα results in attenuation of amyloid deposition in vivo. *Mol Neurodegener* **6**: 16.
33. Chiu, BC, Martin, BE, Stolberg, VR and Chensue, SW (2013). The host environment is responsible for aging-related functional NK cell deficiency. *J Immunol* **191**: 4688–4698.
34. Beers, DR, Henkel, JS, Zhao, W, Wang, J, Huang, A, Wen, S *et al.* (2011). Endogenous regulatory T lymphocytes ameliorate amyotrophic lateral sclerosis in mice and correlate with disease progression in patients with amyotrophic lateral sclerosis. *Brain* **134**(Pt 5): 1293–1314.
35. Butovsky, O, Siddiqui, S, Gabriely, G, Lanser, AJ, Dake, B, Murugaiyan, G *et al.* (2012). Modulating inflammatory monocytes with a unique microRNA gene signature ameliorates murine ALS. *J Clin Invest* **122**: 3063–3087.
36. Zhao, W, Beers, DR, Liao, B, Henkel, JS and Appel, SH (2012). Regulatory T lymphocytes from ALS mice suppress microglia and effector T lymphocytes through different cytokine-mediated mechanisms. *Neurobiol Dis* **48**: 418–428.
37. Boillée, S, Yamanaka, K, Lobsiger, CS, Copeland, NG, Jenkins, NA, Kassiotis, G *et al.* (2006). Onset and progression in inherited ALS determined by motor neurons and microglia. *Science* **312**: 1389–1392.
38. Beers, DR, Henkel, JS, Xiao, Q, Zhao, W, Wang, J, Yen, AA *et al.* (2006). Wild-type microglia extend survival in PU.1 knockout mice with familial amyotrophic lateral sclerosis. *Proc Natl Acad Sci USA* **103**: 16021–16026.
39. Moore, KW, de Waal Malefyt, R, Coffman, RL and O'Garra, A (2001). Interleukin-10 and the interleukin-10 receptor. *Annu Rev Immunol* **19**: 683–765.
40. Yazawa, I, Giasson, BI, Sasaki, R, Zhang, B, Joyce, S, Uryu, K *et al.* (2005). Mouse model of multiple system atrophy alpha-synuclein expression in oligodendrocytes causes glial and neuronal degeneration. *Neuron* **45**: 847–859.
41. Custer, SK, Garden, GA, Gill, N, Rueb, U, Libby, RT, Schultz, C *et al.* (2006). Bergmann glia expression of polyglutamine-expanded ataxin-7 produces neurodegeneration by impairing glutamate transport. *Nat Neurosci* **9**: 1302–1311.
42. Zolotukhin, S, Potter, M, Zolotukhin, I, Sakai, Y, Loiler, S, Fraites, TJ Jr *et al.* (2002). Production and purification of serotype 1, 2, and 5 recombinant adeno-associated viral vectors. *Methods* **28**: 158–167.
43. Geiss, GK, Bumgarner, RE, Birditt, B, Dahl, T, Dowidar, N, Dunaway, DL *et al.* (2008). Direct multiplexed measurement of gene expression with color-coded probe pairs. *Nat Biotechnol* **26**: 317–325.